Calibrationless Multi-Slice Cartesian MRI via Orthogonally Alternating Phase Encoding Direction and Joint Low-Rank Tensor Completion

Yujiao Zhao[1,2†], Zheyuan Yi[1,2,3†], Yilong Liu[1,2],

Fei Chen[3], Linfang Xiao[1,2], Alex T. L. Leong[1,2], and Ed X. Wu[1,2*]

[1]Laboratory of Biomedical Imaging and Signal Processing, the University of Hong Kong, Hong Kong SAR, People's Republic of China,

[2]Department of Electrical and Electronic Engineering, the University of Hong Kong, Hong Kong SAR, People's Republic of China,

[3]Department of Electrical and Electronic Engineering, Southern University of Science and Technology, Shenzhen, People's Republic of China

[*]Correspondence to:

Ed X. Wu, Ph.D.

Department of Electrical and Electronic Engineering

The University of Hong Kong, Hong Kong SAR, China

Tel: (852) 3917-7096

Fax: (852) 3917-8738

Email: ewu@eee.hku.hk

[†]These authors contributed equally to this work

Short Running Title: Calibrationless Multi-slice Cartesian MRI

Total Word Count: 3900 words in main text + 8 main figures + 6 supporting figures

Keywords: Multi-slice, random undersampling, uniform undersampling, phase encoding direction alternation, low-rank tensor completion, calibrationless parallel imaging

Zhao Y, Yi Z, Liu Y, Chen F, Xiao L, Leong ATL, Wu EX. Calibrationless multi-slice Cartesian MRI via orthogonally alternating phase encoding direction and joint low-rank tensor completion. NMR Biomed. 2022 Jul;35(7):e4695. doi: 10.1002/nbm.4695.

Abstract

We propose a multi-slice acquisition with orthogonally alternating phase encoding (PE) direction and subsequent joint calibrationless reconstruction for accelerated multiple individual 2D slices or multi-slice 2D Cartesian MRI. Specifically, multi-slice multi-channel data are first acquired with random or uniform PE undersampling while orthogonally alternating PE direction among adjacent slices. They are then jointly reconstructed through a recently developed low-rank multi-slice Hankel tensor completion (MS-HTC) approach. The proposed acquisition and reconstruction strategy was evaluated with human brain MR data. It effectively suppressed aliasing artifacts even at high acceleration factor, outperforming the existing MS-HTC approach where PE direction is the same among adjacent slices. More importantly, the new strategy worked robustly with uniform undersampling or random undersampling without any consecutive central k-space lines. In summary, our proposed multi-slice MRI strategy exploits both coil sensitivity and image content similarities across adjacent slices. Orthogonally alternating PE direction among slices substantially facilitates low-rank completion process and improves image reconstruction quality. This new strategy is applicable to uniform and random PE undersampling. It can be easily implemented in practice for multiple individual 2D slices Cartesian parallel imaging without any coil sensitivity calibration.

Introduction

In conventional multiple individual 2D slices or multi-slice 2D Cartesian MRI, a series of 2D slices are acquired for a 3D coverage. Here parallel imaging often accelerates single-slice data acquisition by skipping phase encoding (PE) steps in a uniform undersampling pattern. Such undersampling can be easily implemented in practice but causes image domain aliasing that manifests as highly coherent replicas of original image contents. Typical parallel imaging reconstruction methods use coil sensitivity information obtained from extra calibration scans[1] or exploit linear dependency of k-space from sufficient autocalibration signals (ACSs)[2,3].

Recently, low-rank matrix completion has been adopted to exploit low-rank property in structured k-space data for calibrationless reconstruction[4-8]. For example, in simultaneous autocalibrating and k-space estimation (SAKE)[4], single-slice multi-channel k-space data are organized into a block-wise Hankel structured matrix, and the reconstruction is then formulated as a low-rank constraint optimization problem. 1D or 2D random undersampling, in contrast to uniform undersampling, is commonly adopted in these methods because it can introduce incoherency, allowing the aliasing to appear in noise-like pattern[9]. However, for 2D Cartesian MRI, 1D random undersampling enables the aliasing to spread along PE direction only.

Clinical multiple individual 2D slices MR data exhibit strong correlations because coil sensitivity maps vary smoothly and anatomical structures of the scanned subject often change slowly along slice direction. Multiple individual 2D slices acquisition or multi-slice 2D acquisition also potentially offers the flexibility of acquiring different slices with different sampling patterns, through which dedicated sampling schemes can be designed to explore the correlations in multi-slice data. For example, such flexibility has been incorporated with traditional parallel imaging reconstruction methods. With the assumption of adjacent slices sharing similar coil sensitivity maps, ACSs can be acquired from few evenly spread slices, and coil sensitivity maps for other slices are then obtained from adjacent slices through interpolation[10]. Alternatively, in z-GRAPPA[10], each slice is acquired with one PE line shifted from its position in previous slice. Thus ACS acquisition is avoided because the k-space lines from adjacent slices can be combined to form a block of fully sampled data for calibration. In addition, since

adjacent multi-slice images often share similar image contents[11-14], one can acquire adjacent slices with different undersampling factors and then estimate missing k-space data of a highly undersampled slice by interpolating data from neighboring slices[11,12].

The aforementioned sampling schemes have been incorporated with compressed sensing (CS) reconstruction in few preliminary studies to further explore correlations in multi-slice data. A CS based method has been presented for jointly reconstructing multi-slice data by applying a sparsifying transform to both x-y and y-z planes[15,16]. In particular, 1D random undersampling patterns are independently generated for different slices, thus allowing sparsity exploitation in two dimensions. However, 1D random undersampling pattern adopted in this method, as well as in other low-rank based calibrationless reconstruction methods, is non-adaptive because the optimal pattern that maximizes the incoherency depends on acquisition parameters (e.g., acceleration factor or matrix size)[17,18].

In our recent study, we developed a method of joint reconstruction of undersampled multi-slice data through a multi-slice Hankel tensor completion (MS-HTC) framework[19]. The method can effectively reconstruct multi-slice data that are acquired with 2D spiral undersampling patterns varying among adjacent slices. It can also reconstruct undersampled Cartesian multi-slice data acquired with different 1D random PE undersampling patterns (including few consecutive central k-space lines) among slices. Cartesian multi-slice MRI is valuable in clinical settings as it presently constitutes the bulk of the 2D imaging protocols[20-22]. In this study, we aim to further advance this joint multi-slice approach for multiple individual 2D slices Cartesian MRI by introducing orthogonal PE direction alternation among slices during data acquisition. Specifically, multi-channel k-space data for each slice are randomly or uniformly undersampled along PE direction, while the PE direction orthogonally alternates among adjacent slices. Such multi-slice acquisition, together with MS-HTC reconstruction framework, augments the overall incoherency and enables more effective utilization of the coil sensitivity and image content similarities among adjacent slices. Furthermore, this new strategy is applicable to uniform undersampling, thus offering more flexibility in clinical MRI applications.

Methods

Multi-slice data acquisition with orthogonally alternating PE direction

An acquisition scheme with PE direction alternation is proposed for multiple individual 2D slices Cartesian MRI such that coil sensitivity and image content correlations in multi-slice MR data can be more effectively explored in MS-HTC reconstruction to achieve calibrationless reconstruction with high accelerations. As shown in Figure 1, k-space data for each slice are randomly or uniformly undersampled along one PE direction, while undersampled k-space data for the next adjacent slice are acquired with PE along the orthogonal direction. On one hand, due to the relatively slow variation of coil sensitivity maps and anatomical structures, the proposed acquisition scheme enables each slice to utilize complementary information along its undersampling direction from adjacent slices. On the other hand, the proposed acquisition scheme allows aliasing from adjacent slices to spread along two different or orthogonal directions, thus forcing them to be more incoherent and facilitating the low-rank tensor completion process in the joint multi-slice reconstruction. Note that the proposed PE direction alternation can be applied to both random and uniform undersampling. It can be easily implemented in practice by simply swapping PE and frequency encoding (FE) directions among adjacent slices.

Joint reconstruction using MS-HTC

The randomly or uniformly undersampled multi-slice data are jointly reconstructed through low-rank Hankel tensor completion approach using our recently developed MS-HTC framework[19]. As shown in Figure 2, undersampled k-space data from each slice are structured into a block-wise Hankel matrix. The Hankel matrices from multiple adjacent slices are then concatenated along a third dimension, forming a third-order multi-slice tensor ($\boldsymbol{T}$). Higher-order singular value decomposition (HOSVD)[23,24] is then employed to decompose tensor $\boldsymbol{T}$ by deriving a core tensor $\boldsymbol{S}$ and 3 orthogonal bases $U^{(n)}$ (n = 1, 2, and 3),

$$\boldsymbol{T} = \boldsymbol{S} \times_1 U^{(1)} \times_2 U^{(2)} \times_3 U^{(3)} \quad (1)$$

where $\times_n$ is the n-mode product of a tensor and a matrix. Here $U^{(n)}$ is unitary matrix,

which is obtained by performing singular value decomposition (SVD) of the *n*-mode unfolding matrix $T_{(n)}$. A multilinear low-rank approximated tensor, denoted as $\boldsymbol{\Gamma}$, is then derived by rank truncation of the tensor $\boldsymbol{T}$. With the n-mode ranks of $\boldsymbol{T}$ known, the recovery of multi-slice undersampled data (Y) is formulated as

$$\begin{aligned} &\underset{X}{argmin} \, \|DP^{-1}(\boldsymbol{\Gamma}) - Y\|_F^2 \\ &s.t. \; \boldsymbol{\Gamma} \approx \boldsymbol{S} \times_1 U^{(1)} \times_2 U^{(2)} \times_3 U^{(3)} \end{aligned} \tag{2}$$

where D denotes the undersampling operator, and P^{-1} denotes the pseudo-inverse operator that generates multi-slice k-space data (X) from approximated low-rank multi-slice tensor ($\boldsymbol{\Gamma}$).

The implementation of joint reconstruction is illustrated in Figure 2. For k-space data of each slice, a block-wise Hankel matrix is constructed by sliding a multi-channel window across the whole k-space. The 3rd-order multi-slice tensor ($\boldsymbol{T}$) is then formed by concatenating Hankel matrices from multiple adjacent slices. The dimensions D_n (n = 1, 2 and 3) of the multi-slice tensor $\boldsymbol{T} \in \mathbb{C}^{D_1 \times D_2 \times D_3}$ corresponding to k-space samples from different kernels, channels, and slices are termed as kernel, channel, and slice dimensions, respectively. By stacking vectors of multi-slice tensor along its channel, kernel and slice dimensions, unfolding matrices $T_{(1)} \in \mathbb{C}^{D_1 \times D_2 D_3}$, $T_{(2)} \in \mathbb{C}^{D_1 D_3 \times D_2}$ and $T_{(3)} \in \mathbb{C}^{D_1 D_2 \times D_3}$ can be obtained[23], termed as 1-mode, 2-mode, and 3-mode unfolding matrices, respectively. In this work, HOSVD is conducted by performing matrix SVD and rank truncation on $T_{(1)}$ and $T_{(2)}$, through which the image content and coil sensitivity similarities across adjacent slices can be exploited as demonstrated in our recent MS-HTC study[19]. After low-rank tensor approximation and enforcing Hankel structural and data consistency, the k-space data are updated. These steps are repeated iteratively until convergence.

Evaluation by human brain imaging at 3T

In vivo experiments were performed on a Philips Achieva 3T scanner equipped with an 8-channel head coil. All experiments involving human subjects were approved by the local institutional board and written information consents were obtained.

Fully sampled axial T2-weighted (T2w) and T1-weighted (T1w) datasets were acquired

with FOV = 240×240 mm^2, slice thickness/gap = 4/1 mm, matrix size = 240×240, and slice number = 16. T2w dataset was acquired using 2D fast spin echo (FSE) sequence with bandwidth = 59.04 kHz, echo train length (ETL) = 20 and TR/TE = 3000/113 ms. T1w dataset was acquired using 2D spin echo (SE) sequence with bandwidth = 49.68 kHz, TR/TE = 600/10 ms and flip angle = 70°. Each dataset was acquired twice with PE in both left-right (LR) and anterior-posterior (AP) directions, from which one fully sampled test dataset with alternating LR/AP PE direction for odd/even slice was retrospectively synthesized.

Undersampled test datasets with various undersampling factors (Rs) and patterns were then extracted accordingly in a retrospective manner for the proposed LR/AP PE direction alternation or fixed LR PE direction. As shown in Figure S1, random 1D Poisson disk undersampling pattern[25] was independently generated for each slice with (as in our recent study[19]) or without extra 4 consecutive central k-space lines. For uniform undersampling, the same sampling pattern was used for all slices. Given that uniform undersampling with fixed LR PE direction can generate extremely coherent aliasing[26,27], complementary or interleaving uniform undersampling patterns among slices (i.e., shifting by one line from slice to slice) were also generated and evaluated.

All undersampled datasets were jointly reconstructed with the MS-HTC framework. Kernel size was set to 6×6 and target rank was optimized to achieve the best reconstruction performance. Window-normalized rank[4] was 1.5/1.6 for 1-mode/2-mode unfolding with 2-slice reconstruction. The MS-HTC iteration was terminated when the update of k-space data estimation was lower than 0.1‰[19]. Common spatial supports of joint slices were estimated during low-rank completion iterations for evaluation. Specifically, they were computed as sum of square images from null subspace basis, which was extracted through rank truncation of the 2-mode unfolding matrix $T_{(2)}$[28,29]. Final reconstructed images were obtained by combining individual coil images using the square root sum-of-squares (rSOS) method. Reference images were reconstructed from fully sampled data. Residual error maps were calculated by subtracting reconstructed images from reference images channel-by-channel and then combining through rSOS. Peak signal-to-noise ratio (PSNR) and normalized root-mean-square errors (NRMSEs) within the brain region were also measured to assess reconstruction performance.

Image reconstruction algorithm and its evaluation were implemented using MatLab (MathWorks, Natick, MA), and the source code can be obtained online (https://github.com/loyalliu/MS-HTC2) or from the authors upon request.

Results

The joint 2-slice MS-HTC reconstruction results of 8-channel T2w data acquired with and without PE direction alternation are shown in Figure 3. All datasets were randomly or uniformly undersampled at R = 4. The undersampling patterns are depicted in Figure S1. For each undersampled dataset, 2 slices were jointly reconstructed. The corresponding phase images are shown in Figure S2. In general, the reconstruction results of data randomly undersampled with alternating LR/AP PE direction exhibited less aliasing artifacts than those of data randomly undersampled along LR PE direction. In absence of extra 4 central k-space lines, PE direction alternation still enabled successful reconstruction while fixed PE direction approach largely failed, leading to ~0.05 reduction of NRMSEs and ~6dB increase of PSNR. The improvement was more significant when data were uniformly undersampled. With alternating PE direction, artifacts arising from uniform undersampling were effectively suppressed, achieving similar NRMSEs and PSNR as using random undersampling. In contrast, with fixed PE direction, the coherent aliasing led to complete failure of joint reconstruction.

Figures 4 and 5 show the interim common spatial supports and reconstruction results during the 15^{th} joint reconstruction iteration when reconstructing the results in Figure 3. As shown in Figure 4, for both random and uniform undersampling, common 2-slice spatial supports estimated from data with alternating PE direction became comparable to those estimated from fully sampled reference data after only 15 iterations, while those estimated from data with LR PE direction were less compact when compared to reference. Meanwhile, undersampling with alternating PE direction, together with joint reconstruction, allowed the overall aliasing to spread in both directions (see Figures 5A and 5B), including the aliasing leakage in two directions among slices (red arrows). In contrast, undersampling along LR PE direction and joint reconstruction caused the aliasing to spread along one direction only. The proposed acquisition with alternating PE direction greatly facilitated the low-rank Hankel tensor completion process, yielding

faster computational convergence and smaller NRMSEs as shown in Figure 6.

The influence of slice number on joint multi-slice reconstruction for data acquired with PE direction alternation is demonstrated in Figure 7. Eight-channel T2w data were uniformly undersampled at R = 4. Multiple consecutive slices (slice number = 2, 3 and 4) were jointly reconstructed using MS-HTC. The results indicated that joint reconstruction with more slices improved the reconstruction in terms of higher PSNR and smaller NRMSEs. Figures S3 and S4 present the reconstruction results of 8-channel T2w data at R = 3, and T1w data at R = 3 and 4, respectively. They again illustrated that the proposed PE direction alternation strategy was effective and robust for reconstructing uniformly undersampled multi-slice data, and the image quality could be improved through increasing slice number of joint reconstruction.

Figure 8 shows the joint 2-slice reconstruction results of 8-channel T2w data with different gaps between 2 jointly reconstructed slices (i.e., different extents of similarities in coil sensitivity and image content among adjacent slices). Data were uniformly undersampled at R = 4 with PE direction alternating among two slices. By skipping one or two slices, the slice gap between jointly reconstructed slices was increased substantially (i.e., from 1 mm to 6 and 11 mm, respectively). The reconstruction error increased with slice gap due to reduced coil sensitivity and image content similarities.

Discussion

A strategy of multi-slice acquisition with orthogonally alternating PE direction and joint low-rank tensor completion reconstruction is presented here for calibrationless multiple individual 2D slices or multi-slice 2D Cartesian MRI. We have demonstrated that this strategy can effectively suppress aliasing artifacts, outperforming our recently proposed approach[19] that is based on MS-HTC reconstruction but without PE direction alternation. When applied to 1D random PE undersampling, our new approach requires no extra consecutive central k-space lines (i.e., no extra coil sensitivity information). More importantly, it works robustly with uniform undersampling, where many existing low-rank based calibrationless reconstruction methods are problematic due to the lack of incoherency. Therefore, it can be easily incorporated into existing multi-slice

Cartesian MRI protocols such as 2D FSE-based protocols that are widely used in clinical MRI at present time.

In multiple individual 2D slices or multi-slice 2D MRI, adjacent slices share similar coil sensitivity maps due to slow variation of coil sensitivity along slice direction. From parallel imaging point of view, such similarity allows coil sensitivity from one slice to be estimated with ACSs from its adjacent slices[10]. In addition, cross-sampled GRAPPA has demonstrated that aliasing artifacts can be further reduced compared with conventional GRAPPA by swapping PE and FE directions between ACSs and data acquisition, especially when limited ACSs are available[30,31]. This can be explained as that more accurate coil sensitivity estimation requires more ACSs along the undersampled PE direction than the fully sampled FE direction, which can be readily achieved by acquisition with alternating PE direction. This also indicates that, with our proposed PE direction alternation and MS-HTC strategy, each slice can utilize complementary calibration information along its undersampling direction from adjacent slices, leading to more effective exploitation of coil sensitivity similarity among adjacent slices.

Adjacent slices also share similar spatial support due to the smooth variation of object contour along slice direction. As shown in Figure 4, for both random and uniform undersampling, common spatial supports estimated from data with alternating PE direction were more compact when compared with those estimated from data acquired with LR PE direction. They approached those estimated from the fully sampled data after only 15 iterations. This was because spatial support information provided by fully sampled frequency encoding (FE) data at one slice could inherently constrain spatial supports of adjacent slices with FE along the orthogonal directions. Note that low-rank Hankel matrix can be more easily estimated when it is constructed from an image with smaller spatial support[5]. Therefore, with the reduced common spatial supports, less residual artifacts (Figure 3) and faster convergence (Figure 6) were achieved by the proposed strategy.

Our recent work has indicated that the reconstruction performance of MS-HTC can be significantly improved through increasing the incoherency of sampling pattern, as demonstrated by multi-slice spiral acquisition and joint reconstruction[19]. Multi-slice spiral acquisition provides an excellent scenario where different 2D spiral

undersampling patterns can be applied to adjacent slices to significantly increase the incoherency during MS-HTC reconstruction. However, spiral imaging is relatively complex. It is more sensitive to hardware imperfections that cause blurring or distortion on reconstructed images[32,33], and less adopted compared to multi-slice Cartesian acquisition. Multiple individual 2D slices Cartesian MRI is more robust and widely used in clinical settings. In this study, an acquisition scheme of orthogonally alternating PE direction is proposed to significantly improve the overall incoherency across different slices during MS-HTC reconstruction for multiple individual 2D slices Cartesian MRI. The proposed combination of alternating PE direction acquisition and joint MS-HTC reconstruction forces the overall aliasing to occur along two orthogonal directions (Figure 5A), including the aliasing leakages among adjacent but structurally different slices, creating multi-dimensionally incoherent aliasing patterns and thus greatly facilitating the low-rank tensor completion process. This greatly improves the MS-HTC reconstruction for random undersampling[4,6,34,35]. Note that the MS-HTC can be further improved for random undersampling by introducing additional regularization[36] to enforce the sparsity in transform domain.

Furthermore, low-rank matrix completion methods often fail to solve the ill-posed problem when k-space data are uniformly undersampled (see Figure 3 for results from uniformly undersampled T2W data with fixed LR PE direction). This is because uniform undersampling generates artifacts that manifest as replicas of original image contents, such that they will be equally likely to be considered as the solutions for constraint optimization[27,37,38]. Our proposed acquisition and reconstruction strategy mitigated the coherence arising from uniform undersampling by spreading the aliasing into two directions (Figure 5B), thus turning the optimization into a better-posed problem.

The proposed joint reconstruction explores coil sensitivity and image content similarities across adjacent slices. As shown in Figure 7 and Figures S3 and S4, the reconstruction performance was robust for T2w FSE and T1w SE data undersampled at different and high accelerations (R = 3 and 4). With increasing number of jointly reconstructed slices, better reconstruction performance was achieved for both datasets. This was because the multi-slice tensor became more rank-deficient with more jointly reconstructed slices. The similarities between adjacent slices decreased when a larger

slice gap was employed, leading to degraded reconstruction results as expected (Figure 8). In practice, the number of jointly reconstructed slices can be experimentally optimized. The joint reconstruction can also be procedurally incorporated with a sliding window reconstruction strategy to better extract undersampled data from adjacent slices with similar coil sensitivities and image contents, through which the correlations in multi-slice data can be better utilized.

The performance of the proposed acquisition and reconstruction strategy also depends on reconstruction parameters, such as kernel size and target rank. As shown in Figure S5, increasing kernel size slightly improves reconstruction performance. However, a larger kernel size greatly increases computation load[4]. In this perspective, the minimum kernel size that can provide sufficient reconstruction accuracy should be adopted. The selection of target rank is related to many practical factors (e.g., kernel size, the number of jointly reconstructed slices and the similarities in multi-slice data). In this study, that target rank was empirically determined to guarantee the optimal reconstruction results (see reconstruction results with suboptimal target rank in Figure S6). In future studies, automatic rank selection can be investigated.

Alternating PE direction among adjacent slices can introduce slight data inconsistency among slices due to hardware imperfections, such as gradient delays, eddy current, and field inhomogeneity[30,39-41]. As shown in the reference phase images in Figure S2, alternating PE direction could lead to minor phase difference, which was caused mostly by the slight k-space center misalignment when changing PE direction in this case. Nevertheless, for both random and uniform undersampling with alternating PE direction, the aliasing artifacts were still effectively suppressed and the phase images were well reconstructed despite such hardware related phase inconsistency among adjacent slices. In practice, it is possible to implement correction methods to estimate or calibrate, and then correct such minor but undesired data inconsistency for better joint MS-HTC reconstruction performance, particularly for phase-sensitive MRI applications. For example, by assuming slow variation of image phase change between adjacent slices, such phase differences can be extracted and then compensated before constructing the multi-slice tensor. Such correction can also be pursued in an iterative manner.

The data inconsistency among slices may also arise from the T2/T2* decay that can

introduce different k-space weightings to adjacent slices with the proposed acquisition scheme. Figure 3 suggested that the proposed strategy could tolerate such inconsistency for the T2w dataset acquired using 2D FSE sequence with ETL = 20 and matrix size = 240×240. With alternating PE direction, susceptibility induced off-resonance may also cause image distortion along different directions and chemical shift artifacts may also rotate to different directions. The aforementioned data inconsistency may become more significant for echo planar imaging or gradient echo imaging with long TE, which needs to be examined in future studies.

The acceleration of the proposed strategy can be limited for rectangular FOV acquisition, where increasing the number of sampled PE steps for some slices may be required. Another potential limitation is the application with a FOV smaller than the object being imaged, where wrap-around artifacts can occur in PE direction using the proposed acquisition. In addition, the proposed PE direction alternation can cause flow or motion artifacts to spill in two directions, e.g., affecting the regions of diagnostic interest. However, early study has demonstrated that, by acquiring two datasets with alternating PE direction, artifacts due to subject motion or sequence property could be significantly reduced with the assumption of the image contents from two datasets were correlated but the artifacts were not[39]. Future study may examine the utilization of the image content and support similarities among slices to reduce such motion or flow artifacts.

We conducted the proposed joint reconstruction using a personal desktop computer equipped with 4-core i5-6500 CPU and 16-GB RAM. For 8-channel T2w data acquired with matrix size = 240×240 and undersampled at R = 4, the convergence of joint reconstruction with kernel size = 6×6 took about 35, 50 and 60 minutes for 2-slice, 3-slice and 4-slice reconstruction, respectively. Most of the reconstruction time was consumed by the tensor decomposition, tensor construction and recovering k-space data from the approximated tensor. Thus the reconstruction time will increase if larger matrix size or kernel size is employed. To improve the computation efficiency, the joint reconstruction can be potentially incorporated with efficient low-rank approximation methods[42,43], image-space reconstruction by structured low-rank tensor estimation of coil sensitivity and spatial support[29], or implemented with high-performance GPU-based computing.

Conclusion

This study presents a multi-slice acquisition and joint reconstruction strategy for accelerating multiple individual 2D slices or multi-slice 2D Cartesian MRI. It acquires multi-slice undersampled data with orthogonally alternating PE direction among adjacent slices and then jointly reconstructs all slices through low-rank Hankel tensor completion. This new strategy not only exploits the coil sensitivity and image content similarities across adjacent slices but also substantially augments incoherency, which consequently facilitates the low-rank completion process and improves the MS-HTC image reconstruction quality. Furthermore, this strategy works robustly with uniform undersampling as well as random undersampling in absence of extra consecutive central k-space lines. Thus it can be readily implemented in practice to enable multiple individual 2D slices Cartesian parallel imaging without any coil sensitivity calibration.

Acknowledgments

This study is supported in part by Hong Kong Research Grant Council (R7003-19/C7048-16G/HKU17112120 to E.X.W. and HKU17103819/HKU17104020 to A.T.L.), Guangdong Key Technologies for Treatment of Brain Disorders (2018B030332001 to E.X.W.), and Guangdong Key Technologies for Alzheimer's Disease Diagnosis and Treatment (2018B030336001 to E.X.W.).

Reference

[1] Pruessmann KP, Weiger M, Scheidegger MB, Boesiger P. SENSE: sensitivity encoding for fast MRI. Magn Reson Med 1999;42(5):952-962.

[2] Sodickson DK, Manning WJ. Simultaneous acquisition of spatial harmonics (SMASH): fast imaging with radiofrequency coil arrays. Magn Reson Med 1997;38(4):591-603.

[3] Griswold MA, Jakob PM, Heidemann RM, Nittka M, Jellus V, Wang J, Kiefer B, Haase A. Generalized autocalibrating partially parallel acquisitions (GRAPPA). Magn Reson Med 2002;47(6):1202-1210.

[4] Shin PJ, Larson PE, Ohliger MA, Elad M, Pauly JM, Vigneron DB, Lustig M. Calibrationless parallel imaging reconstruction based on structured low-rank matrix completion. Magn Reson Med 2014;72(4):959-970.

[5] Haldar JP. Low-rank modeling of local k-space neighborhoods (LORAKS) for constrained MRI. IEEE Trans Med Imaging 2014;33(3):668-681.

[6] Haldar JP, Zhuo J. P-LORAKS: Low-rank modeling of local k-space neighborhoods with parallel imaging data. Magn Reson Med 2016;75(4):1499-1514.

[7] Lee D, Jin KH, Kim EY, Park SH, Ye JC. Acceleration of MR parameter mapping using annihilating filter-based low rank hankel matrix (ALOHA). Magn Reson Med 2016;76(6):1848-1864.

[8] Lee J, Jin KH, Ye JC. Reference-free single-pass EPI Nyquist ghost correction using annihilating filter-based low rank Hankel matrix (ALOHA). Magn Reson Med 2016;76(6):1775-1789.

[9] Feng L, Benkert T, Block KT, Sodickson DK, Otazo R, Chandarana H. Compressed sensing for body MRI. J Magn Reson Imaging 2017;45(4):966-987.

[10] Honal M, Bauer S, Ludwig U, Leupold J. Increasing efficiency of parallel imaging for 2D multislice acquisitions. Magn Reson Med 2009;61(6):1459-1470.

[11] Pang Y, Zhang X. Interpolated compressed sensing MR image reconstruction using neighboring slice k-space data. In: Proceedings of the 20th Annual Meeting of ISMRM, Melbourne, Australia, 2012, p 2275.

[12] Pang Y, Zhang X. Interpolated compressed sensing for 2D multiple slice fast MR imaging. PLoS One 2013;8(2):e56098.

[13] Weizman L, Rahamim O, Dekel R, Eldar YC, Ben-Bashat D. Exploiting similarity in adjacent slices for compressed sensing MRI. In: Conf Proc IEEE Eng Med Biol Soc, 2014, IEEE, p 1549-1552.

[14] Hirabayashi A, Inamuro N, Mimura K, Kurihara T, Homma T. Compressed sensing MRI using sparsity induced from adjacent slice similarity. In: Conf Proc IEEE Samp TA, 2015, IEEE, p 287-291.

[15] Lustig M, Donoho D, Pauly JM. Multi-slice compressed sensing imaging. In: Proceedings of the 15th Annual Meeting of ISMRM, Berlin, Germany, 2007, p 828.

[16] Lustig M, Donoho D, Pauly JM. Sparse MRI: The application of compressed sensing for rapid MR imaging. Magn Reson Med 2007;58(6):1182-1195.

[17] Ravishankar S, Bresler Y. Adaptive sampling design for compressed sensing MRI. In: Conf Proc IEEE Eng Med Biol Soc, 2011, IEEE, p 3751-3755.

[18] Vasanawala S, Murphy M, Alley MT, Lai P, Keutzer K, Pauly JM, Lustig M. Practical parallel imaging compressed sensing MRI: Summary of two years of experience in accelerating body MRI of pediatric patients. In: Proc IEEE Int Symp Biomed Imaging, 2011, IEEE, p 1039-1043.

[19] Liu Y, Yi Z, Zhao Y, Chen F, Feng Y, Guo H, Leong ATL, Wu EX. Calibrationless parallel imaging reconstruction for multislice MR data using low-rank tensor completion. Magn Reson Med 2020;85(2):897-911.

[20] Madhuranthakam AJ, Yu H, Shimakawa A, Busse RF, Smith MP, Reeder SB, Rofsky NM, Brittain JH, McKenzie CA. T2-weighted 3D fast spin echo imaging with water–fat separation in a single acquisition. J Magn Reson Imaging 2010;32(3):745-751.

[21] Ahmad R, Xue H, Giri S, Ding Y, Craft J, Simonetti OP. Variable density incoherent spatiotemporal acquisition (VISTA) for highly accelerated cardiac MRI. Magn Reson Med 2015;74(5):1266-1278.

[22] Baert A. Parallel imaging in clinical MR applications: Springer Science & Business Media; 2007.

[23] De Lathauwer L, De Moor B, Vandewalle J. A multilinear singular value decomposition. SIAM journal on Matrix Analysis and Applications 2000;21(4):1253-1278.

[24] Kolda TG, Bader BW. Tensor decompositions and applications. SIAM review 2009;51(3):455-500.

[25] Bridson R. Fast Poisson disk sampling in arbitrary dimensions. SIGGRAPH sketches 2007;10:1.

[26] Kanatsoulis CI, Fu X, Sidiropoulos ND, Akcakaya M. Tensor Completion From Regular Sub-Nyquist Samples. IEEE Trans Signal Processing 2020;68:1-16.

[27] Lobos RA, Kim TH, Hoge WS, Haldar JP. Navigator-Free EPI Ghost Correction With Structured Low-Rank Matrix Models: New Theory and

Methods. IEEE Trans Med Imaging 2018;37(11):2390-2402.

[28] Ongie G, Jacob M. Super-resolution MRI using finite rate of innovation curves. In: Proc IEEE Int Symp Biomed Imaging, 2015, IEEE, p 1248-1251.

[29] Yi Z, Zhao Y, Liu Y, Gao Y, Chen F, Wu EW. Fast Calibrationless Image-space Reconstruction by Structured Low-rank Tensor Estimation of Coil Sensitivity and Spatial Support. In: Proceedings of the 29th Annual Meeting of ISMRM, 2021, p 0067.

[30] Wang H, Liang D, King KF, Nagarsekar G, Chang Y, Ying L. Improving GRAPPA using cross-sampled autocalibration data. Magn Reson Med 2012;67(4):1042-1053.

[31] Wang H, Liang D, King KF, Nagarsekar G, Ying L. Cross-sampled GRAPPA for parallel MRI. In: Conf Proc IEEE Eng Med Biol Soc, 2010, IEEE, p 3325-3328.

[32] Tan H, Meyer CH. Estimation of k-space trajectories in spiral MRI. Magn Reson Med 2009;61(6):1396-1404.

[33] Brodsky EK, Samsonov AA, Block WF. Characterizing and correcting gradient errors in non-cartesian imaging: are gradient errors linear time-invariant (LTI)? Magn Reson Med 2009;62(6):1466-1476.

[34] Otazo R, Candes E, Sodickson DK. Low-rank plus sparse matrix decomposition for accelerated dynamic MRI with separation of background and dynamic components. Magn Reson Med 2015;73(3):1125-1136.

[35] Jacob M, Mani MP, Ye JC. Structured Low-Rank Algorithms: Theory, Magnetic Resonance Applications, and Links to Machine Learning. IEEE Signal Processing Magazine 2020;37(1):54-68.

[36] Otazo R, Candes E, Sodickson DK. Low-rank plus sparse matrix decomposition for accelerated dynamic MRI with separation of background and dynamic components. Magn Reson Med 2015;73(3):1125-1136.

[37] Candes EJ, Plan Y. Matrix completion with noise. Proceedings of the IEEE 2010;98(6):925-936.

[38] Klopp O. Noisy low-rank matrix completion with general sampling distribution. Bernoulli 2014;20(1):282-303.

[39] Kruger DG, Slavin GS, Muthupillai R, Grimm RC, Riederer SJ. An orthogonal correlation algorithm for ghost reduction in MRI. Magn Reson Med 1997;38(4):678-686.

[40] Peters DC, Derbyshire JA, McVeigh ER. Centering the projection reconstruction trajectory: reducing gradient delay errors. Magn Reson Med 2003;50(1):1-6.

[41] Cui X, Gore JC, Welch EB. K-space shift correction using an alternating

gradient readout acquisition for improved radial fat-water MRI. In: Proceedings of the 20th Annual Meeting of ISMRM, Melbourne, Australia, 2012, p 2406.

[42] Ongie G, Jacob M. A fast algorithm for convolutional structured low-rank matrix recovery. IEEE Trans Computational Imaging 2017;3(4):535-550.

[43] Haldar JP, Hernando D. Rank-constrained solutions to linear matrix equations using powerfactorization. IEEE Signal Processing Letters 2009;16(7):584-587.

Figure Captions

Figure 1. The proposed acquisition scheme with orthogonally alternating PE direction for multiple individual 2D slices Cartesian MRI. The green and red datasets represent the slices acquired with phase encoding (PE) along left-right (LR) and anterior-posterior (AP) directions, respectively. K-space data for each slice are randomly or uniformly undersampled along one PE direction, while data for the next adjacent slice are undersampled with PE along the orthogonal direction.

Figure 2. Illustration of the joint multi-slice Hankel tensor completion (MS-HTC) reconstruction procedure of multiple individual 2D slices Cartesian undersampled data. MS-HTC is applicable to reconstruction of multi-slice Cartesian data where PE direction alternates or remains the same among slices. Within each iteration: constructing Hankel matrix through a sliding window for each slice, and concatenating multi-slice Hankel matrices to form a 3rd-order tensor; decomposing the multi-slice tensor by deriving a core tensor $\boldsymbol{S}$ and unitary matrices $U^{(1)}$, $U^{(2)}$ and $U^{(3)}$ using higher-order singular value decomposition; low-rank approximation by performing singular value decomposition and rank truncation on 1-mode and 2-mode unfolding matrices $T_{(1)}$ and $T_{(2)}$, and enforcing Hankel structural and data consistency.

Figure 3. Two-slice joint MS-HTC reconstruction results of undersampled T2w FSE data (R = 4) with alternating LR/AP PE direction versus fixed LR PE direction among 2 slices. Datasets were acquired with an 8-channel head coil and slice thickness/gap = 4/1 mm. Reconstruction performance quantified in PSNR and NRMSEs are shown in dB and percentages, respectively. (**A**) For random undersampling, sampling patterns included 1D Poisson disk random patterns varying among 2 slices with or without extra 4 central k-space lines (see Figure S1). With the proposed PE direction alternation, results generally exhibited less aliasing artifacts than those with fixed LR PE direction. Without extra central k-space lines, alternating PE direction still enabled satisfactory reconstruction. (**B**) For uniform undersampling with or without interleaving patterns in 2 slices (see Figure S1), strong aliasing artifacts were apparent with fixed LR PE direction, but effectively suppressed by the proposed PE direction alternation.

Figure 4. Interim common spatial supports at the 15th iteration during reconstruction of the 2-slice T2w image sets shown in Figure 3. For both random and uniform

undersampling, common spatial supports estimated from data with alternating PE direction became more comparable to those from fully sampled data after only 15 iterations.

Figure 5. Interim image reconstruction results at the 15th iteration during reconstruction of the 2-slice T2w image sets shown in Figure 3. The proposed PE direction alternation spread the overall aliasing in two directions during MS-HTC reconstruction, in contrast to one direction in case of fixed LR PE direction, in both (**A**) random undersampling and (**B**) uniform undersampling.

Figure 6. Convergence curves during the joint reconstruction of the 2-slice T2w image sets in Figure 3. For all random and uniform undersampling patterns, the proposed PE direction alternation led to faster convergence and smaller NRMSEs compared to fixed PE direction.

Figure 7. Reconstruction of T2w FSE data with different number of jointly reconstructed slices. Data were acquired with PE direction alternation, slice thickness/gap = 4/1 mm, fixed uniform undersampling for all slices at R = 4, and an 8-channel coil. Different number of slices (slice number = 2, 3 and 4) were jointly reconstructed. The reconstruction performance improved with the increasing of slice number. More results are shown in Figures S3 and S4.

Figure 8. Reconstruction of T2w FSE data with different slice gaps (slice gaps = 1, 6 and 11 mm). Data were acquired with PE direction alternation, fixed uniform undersampling for 2 slices and R = 4, and an 8-channel coil. Four slices were jointly reconstructed, and only two slices are displayed. The extent of similarities in coil sensitivity and image content among adjacent slices reduced with slice gap. This led to slightly larger reconstruction errors as expected.

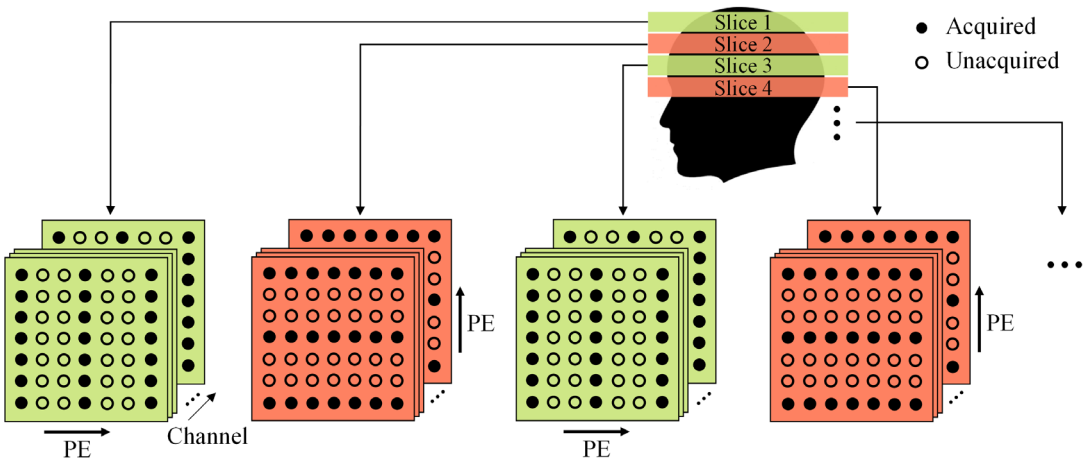

Figure 1

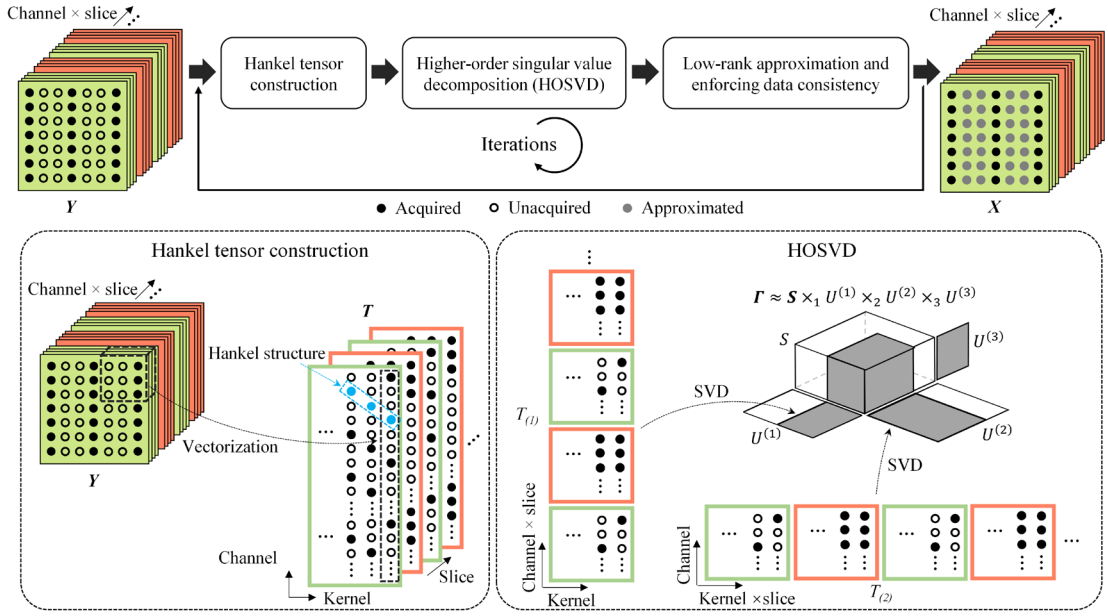

Figure 2

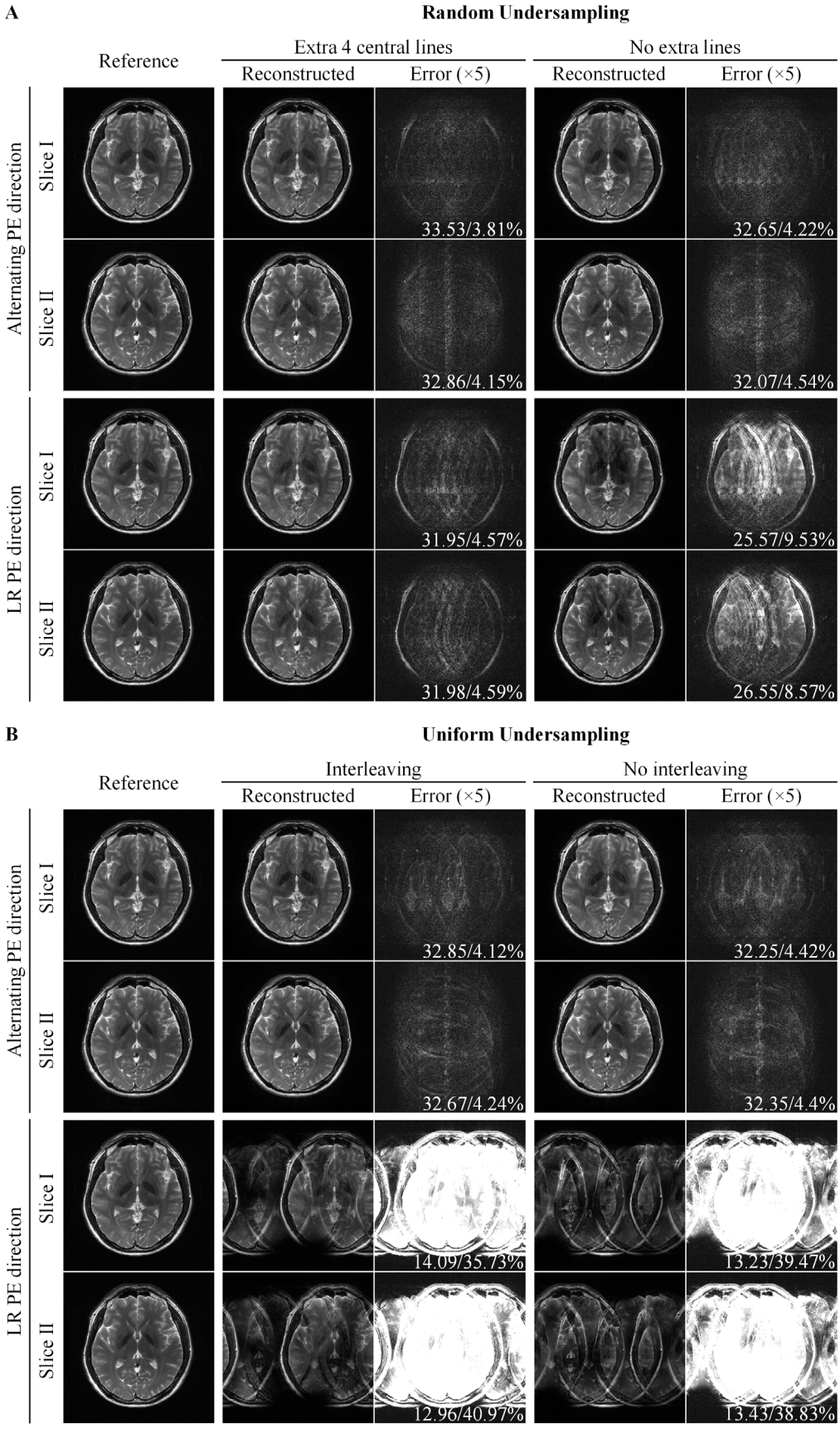
A
Random Undersampling
Reference
Extra 4 central lines
Reconstructed
Error (×5)
No extra lines
Reconstructed
Error (×5)
Alternating PE direction
Slice I
Slice II
LR PE direction
Slice I
Slice II
33.53/3.81%
32.65/4.22%
32.86/4.15%
32.07/4.54%
31.95/4.57%
25.57/9.53%
31.98/4.59%
26.55/8.57%
B
Uniform Undersampling
Reference
Interleaving
Reconstructed
Error (×5)
No interleaving
Reconstructed
Error (×5)
Alternating PE direction
Slice I
Slice II
LR PE direction
Slice I
Slice II
32.85/4.12%
32.25/4.42%
32.67/4.24%
32.35/4.4%
14.09/35.73%
13.23/39.47%
12.96/40.97%
13.43/38.83%

Figure 3

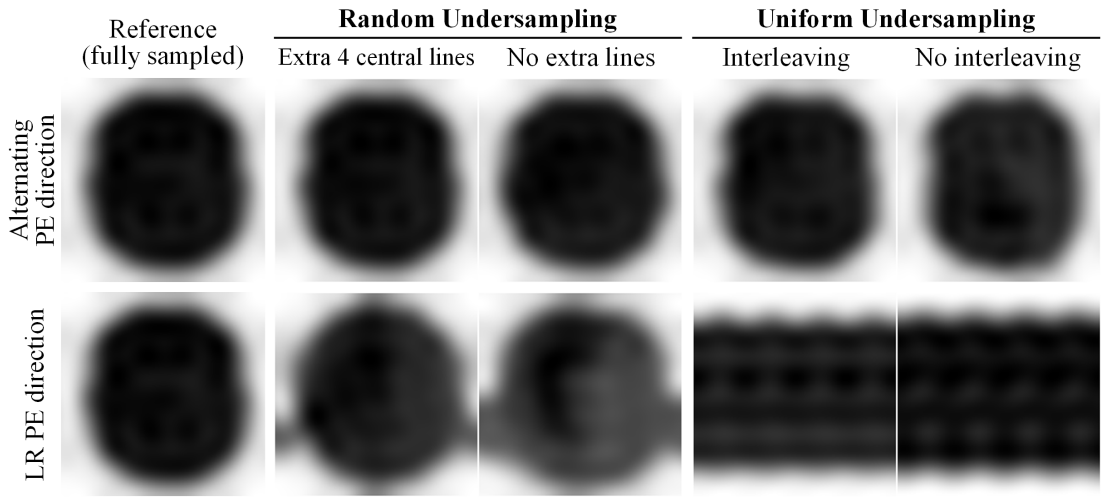
Reference
(fully sampled)
Random Undersampling
Extra 4 central lines
No extra lines
Uniform Undersampling
Interleaving
No interleaving
Alternating
PE direction
LR PE direction

Figure 4

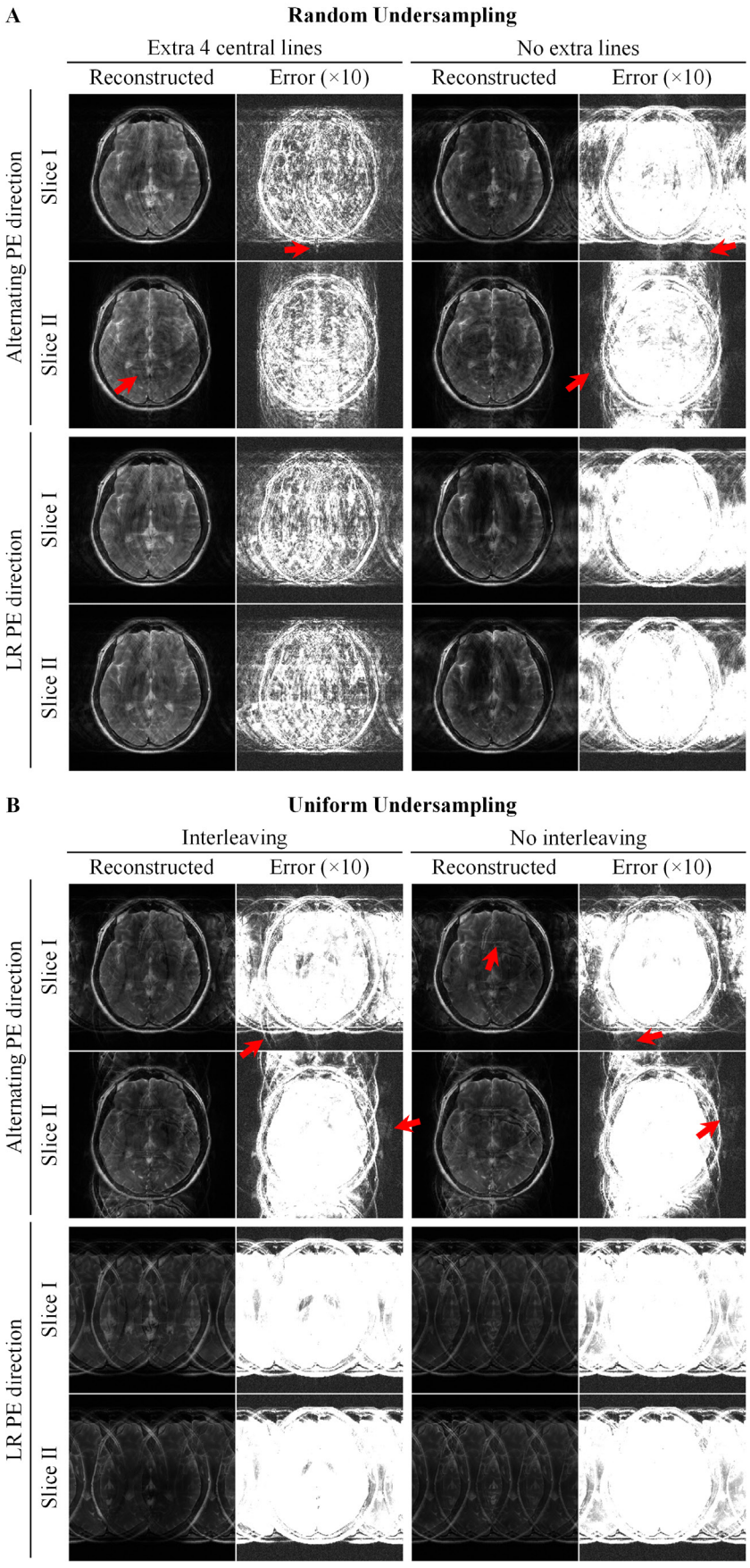
A
Random Undersampling
Extra 4 central lines
No extra lines
Reconstructed
Error (×10)
Reconstructed
Error (×10)
Alternating PE direction
Slice I
Slice II
LR PE direction
Slice I
Slice II
B
Uniform Undersampling
Interleaving
No interleaving
Reconstructed
Error (×10)
Reconstructed
Error (×10)
Alternating PE direction
Slice I
Slice II
LR PE direction
Slice I
Slice II

Figure 5

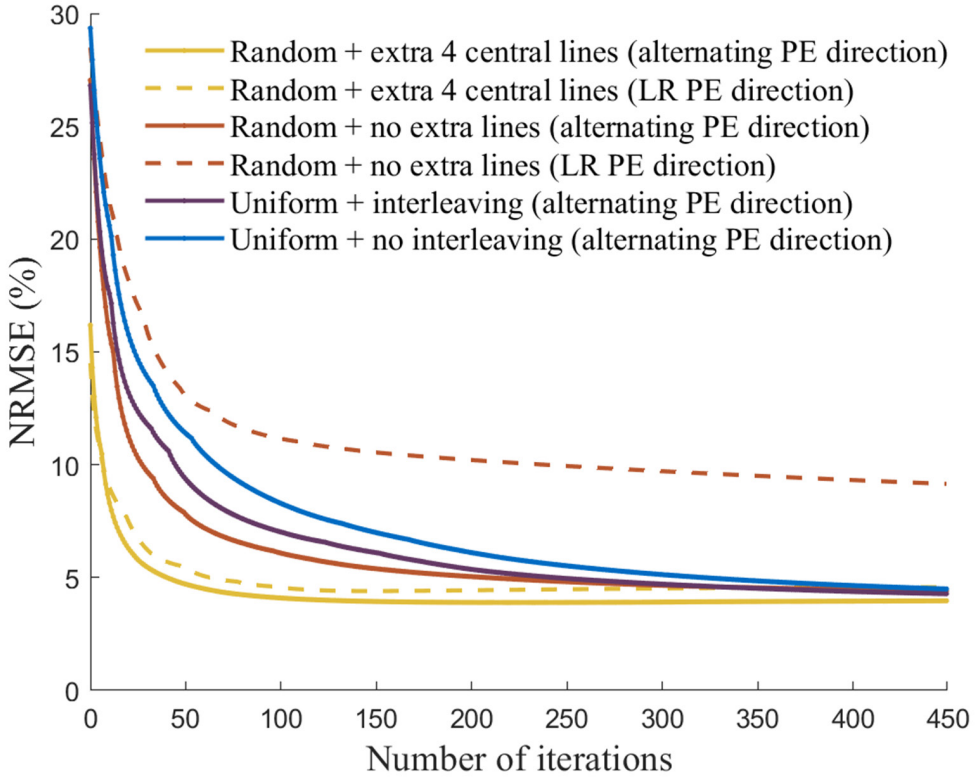
Random + extra 4 central lines (alternating PE direction)
Random + extra 4 central lines (LR PE direction)
Random + no extra lines (alternating PE direction)
Random + no extra lines (LR PE direction)
Uniform + interleaving (alternating PE direction)
Uniform + no interleaving (alternating PE direction)
NRMSE (%)
Number of iterations
0
5
10
15
20
25
30
0
50
100
150
200
250
300
350
400
450

Figure 6

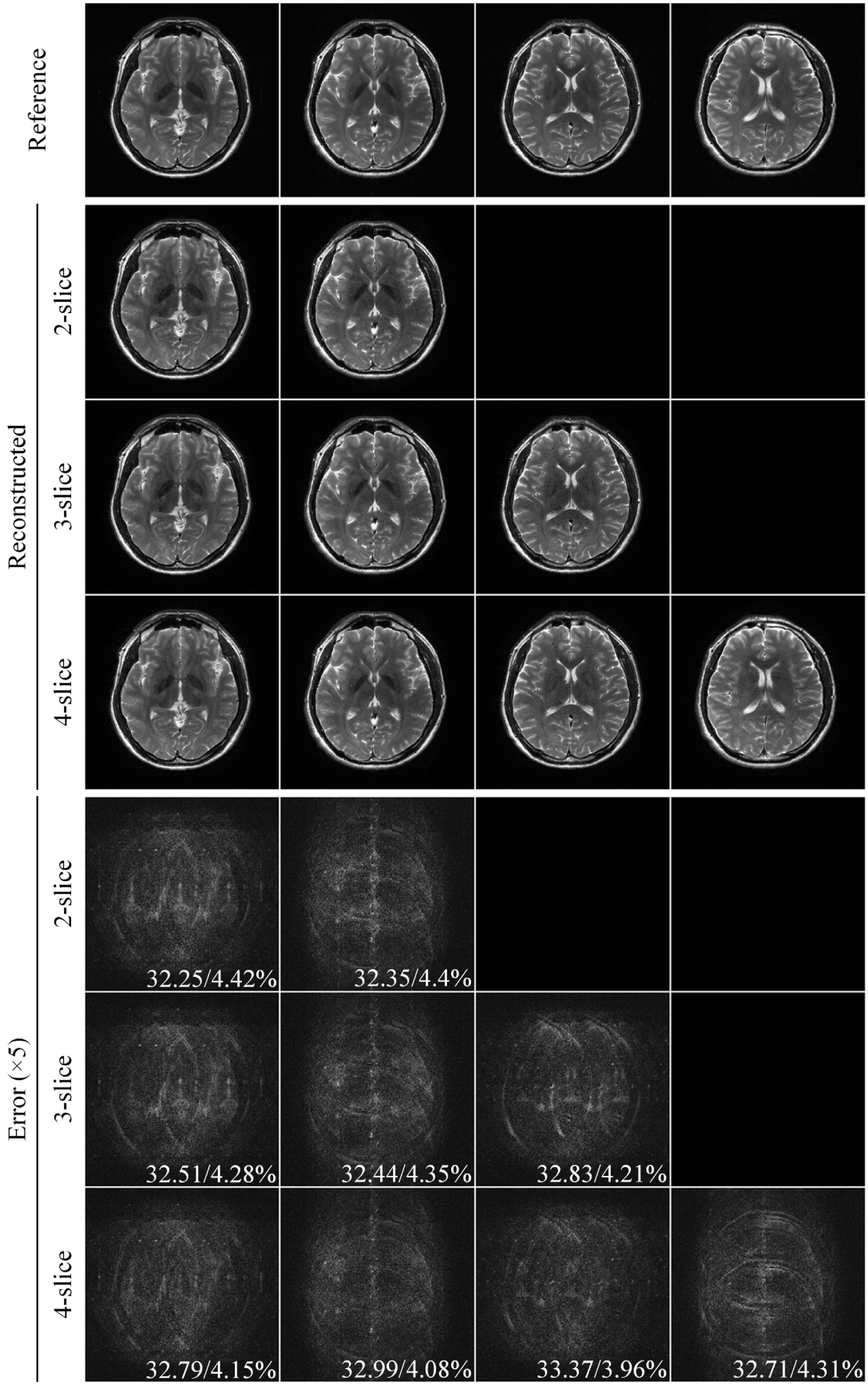
Reference
Reconstructed
2-slice
3-slice
4-slice
Error (×5)
2-slice
3-slice
4-slice
32.25/4.42%
32.35/4.4%
32.51/4.28%
32.44/4.35%
32.83/4.21%
32.79/4.15%
32.99/4.08%
33.37/3.96%
32.71/4.31%

Figure 7

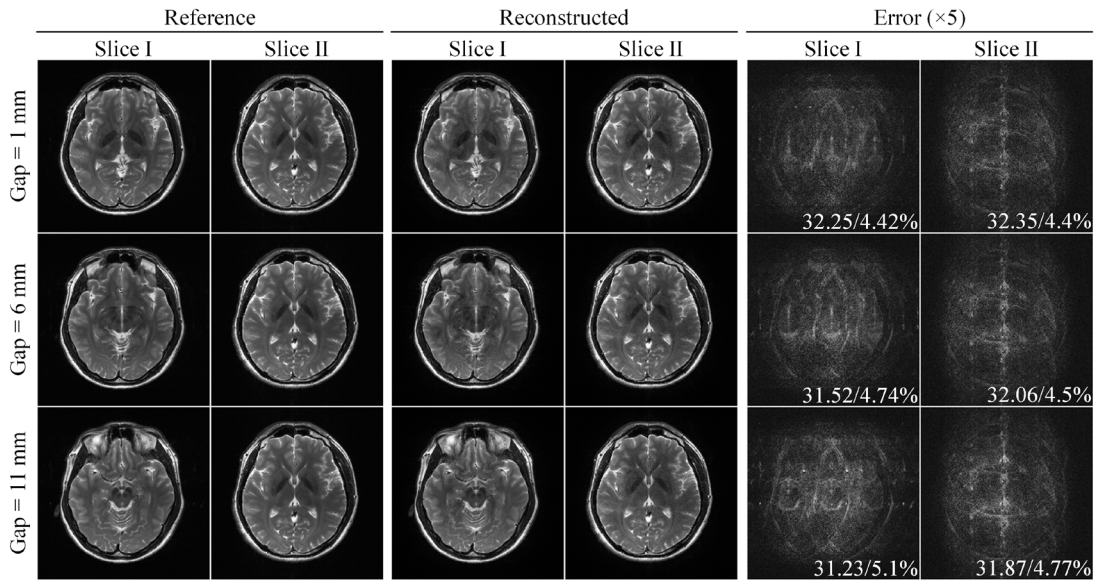
Reference
Reconstructed
Error (×5)
Slice I
Slice II
Slice I
Slice II
Slice I
Slice II
Gap = 1 mm
Gap = 6 mm
Gap = 11 mm
32.25/4.42%
32.35/4.4%
31.52/4.74%
32.06/4.5%
31.23/5.1%
31.87/4.77%

Figure 8